www.czasopisma.pan.pl PAN POLSKA AKADEMIA NAUK www.journals.pan.pl

Arch. Metall. Mater. **67** (2022), 3, 1167-1178

DOI: https://doi.org/10.24425/amm.2022.139717

B. HADAŁA[1], Z. MALINOWSKI[1], A. GOŁDASZ[2], A. CEBO-RUDNICKA[1*]

INVERSE SOLUTION TO THE VERTICAL PLATE COOLING BY RADIATION AND CONVECTION IN AIR

The inverse solution to the heat flux identification during the vertical plate cooling in air has been presented. The developed solution allowed to separate the energy absorbed by the chamber due to radiation from the convection heat losses to air. The uncertainty tests were carried out and the accuracy of the solution has been estimated at a level of 1%-5% depending on the boundary condition model. The inverse solution was obtained for the temperature measurements in the vertical plate. The stainless-steel plate was heated to 950°C and then cooled in the chamber in air only to about 30°C. The identified heat transfer coefficient was compared with the Churchill and Chu model. The solution has allowed to separate the radiation heat losses and to determine the Nusselt number values that stay in good agreement with the Churchill and Chu model for a nearly steady-state air flow for the plate temperature below 100°C.

Keywords: convection heat transfer; radiation heat transfer; plate emissivity; vertical plate

1. Introduction

Cooling in air is one of the essential processes that take place during the steel making processes. It occurs during the hot forging, rolling or continuous casting processes. To simulate such processes the heat transfer boundary conditions should be known, which are a part of the complex models determining properties of products [1]. The cooling of steel products in air from high temperatures reaching of 1200°C involves two mechanism of heat transfer: radiation and convection which depend on the surface temperature. The parameter that influences on the radiation heat transfer is the emissivity of steel surface that depends on the oxide type and structure [2,3]. The problem is less important in the case of stainless steels because during heating its surface is covered with stable Cr_2O_3 oxides which protect steel from further oxidation to the temperature reaching 1100°C [2]. In the case of carbon steels, the problem is more complex because on the surfaces different type of oxides are firmed (FeO, Fe_3O_4 and Fe_2O_3), which are not stable. It changes steel emissivity during the cooling process with temperature and time [3]. Thus, the determination of the radiation and convection heat losses become more complicated. For that reason, the boundary condition determination and implementation in practices is still under development.

The numerical simulations of technological processes including air cooling require the heat transfer boundary conditions which are a part of more complex models determining properties of products [1]. In the literature on the subject, various models are available from the simplest ones giving constant values of the heat transfer coefficient ranging from 10 W/(m^2·K) Puschmann et al. [4] to 20 W/(m^2·K) Bai et al. [5] to more complex, which define convection heat losses based on the Nusselt-Rayleigh relation [6]-[8]. Another kind of models are the ones defining the effective heat transfer coefficient, Malinowski et al. [9] or Devadas et al. [10]. These types of models include the convection heat losses in the emissivity coefficient and because of that the effective emissivity coefficient can be higher than one. Unfortunately, such models have limited implementations to a particular grade of steel and a type of air flow. Much more possibilities provide models allowing to separate heat losses into the convection and radiation part. However, such modes require knowledge about the surface emissivity and the convection heat transfer coefficient (HTC). The convection HTC models were developed based on experimental studies. The formulas defining the Nusselt number Nu differ in form or in the coefficients resulting from the approximation of the experimental data. One of the first Nusselt-Rayleigh (Nu-Ra) relationship have been proposed by Eckert and Jackson [11] and McAdams [12]. Depending on

[1] AGH UNIVERSITY OF SCIENCE AND TECHNOLOGY, FACULTY OF METALS ENGINEERING AND INDUSTRIAL COMPUTER SCIENCE, DEPARTMENT OF HEAT ENGINEERING AND ENVIRONMENT PROTECTION, AL. MICKIEWICZA 30, 30-059 KRAKÓW, POLAND
[2] AGH UNIVERSITY OF SCIENCE AND TECHNOLOGY, FACULTY OF ENERGY AND FUELS, AL. MICKIEWICZA 30, 30-059 KRAKÓW, POLAND
* Corresponding author: cebo@agh.edu.pl

the type of flow and the fluid properties the coefficients in the Nu-Ra formula can differ significantly. Shaub et al. [13] have performed experiments on the copper plate 2 m tall heated to a maximum temperature of 90°C. The plate was polished to minimize emissivity. The experimental data were corrected for the radiation heat losses. The Ra number was in the range from 10^6 to 10^{10}. The results have been compared to the Churchill and Chu model valid for laminar and turbulent flows characterized by the Ra number ranging from 10^{-1} to 10^{12} [14]. The experiments performed by Shaub et al. [13] have shown a mean absolute deviation of 8.1% to the Churchill and Chu model for the isothermal case. For the unsteady experiments, an increase of 22% in the heat transfer was observed in comparison to the quasi-stationary approach. It is an important observation for modelling the transient cooling processes which has indicated that implementation of the empirical Nu-Ra correlation not necessarily leads to satisfactory results for product cooling in the metal industry. It is caused by the fact, that during the product cooling from high temperatures unsteady heat transfer takes place and the convection heat losses can be essentially higher. The model defining the effective Nusselt number as a sum of the convection and radiation heat losses was proposed by Kang Cao et al. [15]. However, the same problem of the limited applicability exists too.

To model temperature changes inside the solid body, a boundary condition describing two heat transfer mechanisms occurring on the surface of this body need to be provided. It is a complex boundary condition including convection and radiation heat transfer. In the paper a model allows to determine the heat losses resulting from free convection on a cooled vertical plate in the temperature range characteristic for metallurgical processes is presented. The model was developed based on the inverse solution, which allowed for separation of heat losses due to radiation and determination of the value of Nu number. Such a solution has not been yet used for cooling in air. The separation of these two heat transfer mechanisms allows the application of the convective boundary condition, regardless of the thermal properties of the surface, i.e. the emissivity, and the influence of the environmental condition on the transfer of thermal energy resulting from radiation. The boundary conditions determined in this way are of particular importance in case of modelling the assumed production processes of metallurgical products.

2. Experimental setup

The determination of the heat flux or HTC at the boundary surface is possible based on the temperature measurements of a cooled object. The plate made of EN 1.4724 steel was heated in the electrical furnace to 950°C. The plate was cooled after heating in the vertical position in the chamber as was shown in Fig. 1. The plate thickness was h = 12 mm, height l = 145 mm and length b = 245 mm. The plate temperature was measured by 9 thermocouples inserted to a depth of 2 mm. The location of thermocouples has been illustrated in Fig. 1. The coordinates of the thermocouple tips have been given in TABLE 1.

TABLE 1

The location of the thermocouple's tips in the plate

Coordinate	T_1	T_2	T_3	T_4	T_5	T_6	T_7	T_8	T_9
x_1, mm	4	4	4	4	4	4	4	4	4
x_2, mm	0	45	90	0	45	90	0	45	90
x_3, mm	30	30	30	72.5	72.5	72.5	115	115	115

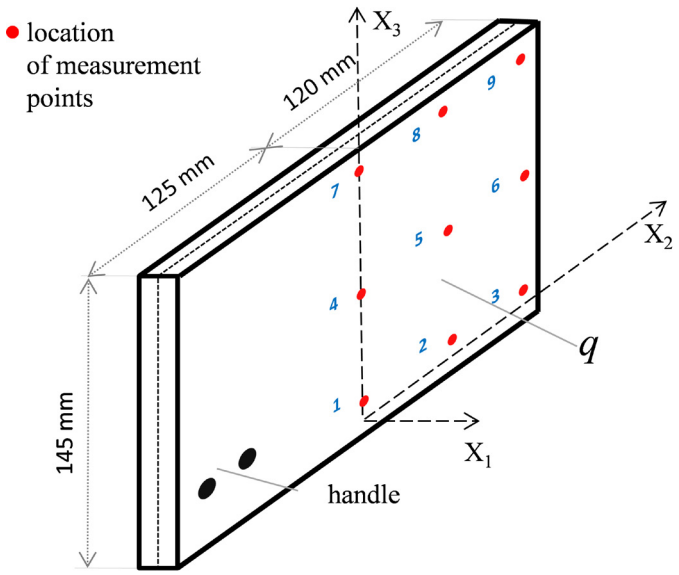

Fig. 1. The location of thermocouples 2 mm below the plate surface

The scheme of the experimental setup has been shown in Fig. 2. The experimental stand consists of an electrical furnace,

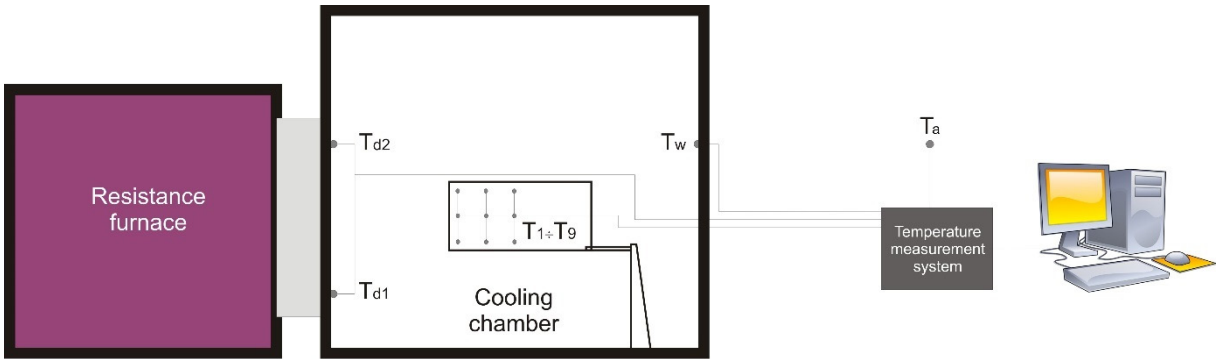

Fig. 2. Scheme of the plate heating and cooling setup

a cooling chamber, and a data acquisition system. Measurements were recorded at a frequency of 1 Hz by a data acquisition system equipped with a noise reduction filter. The furnace temperature was automatically controlled. The measurement system allows collecting data concerning the furnace temperature, the air and chamber temperatures and the plate temperature at selected points. The plate was heated to about 950°C and kept in the furnace approximately 30 minutes to equalize the plate temperature. After that, the plate was moved automatically into the cooling chamber. This process and the furnace door closing were required about 5 seconds. For the temperature measurements the K type thermocouples 1 mm in diameter were employed. The accuracy of the thermocouples was ±0.4% of the measured temperature. The maximum error of the thermocouple at temperature of 1000°C was about ±4°C. In addition to that an error of ±2°C could result from the gauge accuracy connecting thermocouples to the data acquisition system. Thus, based on the accuracy specified by the producers the maximum error of the measured temperature was about 4.5°C.

The plate temperature variations during cooling in the chamber in air only have been given in Fig. 3. The plate temperature at the thermocouple locations was similar, however some differences were observed. The plate temperature after heating was not even and varied from 947.3°C at T_1 to 956.3°C at T_9 thermocouple. The difference partly resulted from uneven heating and to some extend from the temperature measurement errors. After 1000 s of cooling the plate temperature has dropped to 264.1°C at T_3 and to 294.4°C at T_7 thermocouple. The temperature difference resulted mainly from uneven cooling, developed over the plate surface. At the end of cooling after 7000 s the plate temperature has dropped to 32.6°C at T_3 and to 33.4°C at T_4 thermocouple. At the end of cooling the plate temperature was the highest at the center and the lowest at the corner of the plate. Thus, the plate temperature distribution can be considered as typical for this type of cooling.

During cooling the air and chamber temperatures were recorded and have been shown in Fig. 4. The air temperature T_a outside the chamber was about 20.5°C. The chamber walls temperature was recorded at 3 points. The T_w point was located at the wall parallel to the plate surface approximately in the center of the wall. The points T_{d1} and T_{d2} were located at the wall separating the cooling chamber from the electrical furnace. The point T_{d1} was located below the plate and the point T_{d2} above the plate. The chamber temperature was varied during the plate cooling. At the beginning of cooling the chamber temperature was 20.5°C. The chamber walls collected heat from the plate and after 700 s the chamber walls temperature was the highest. At the point T_w temperature of 37°C was reached. The highest wall temperature of 52.5°C was recorded above the plate at the T_{d2} point. Below the plate the wall temperature was slightly lower and 46.5°C at the T_{d1} point was reached.

The temperature measurement errors resulting from using thermocouples were simulated with the finite element method (FEM). In the FEM model the thermocouple structure and the thermophysical properties of the thermocouple were simplified. The thermocouple was modeled as a square bar 1 mm in the cross section inserted to a depth of 2 mm. Four elements with the linear shape functions were employed in the thermocouple's cross section. The properties of the material simulating the thermocouple were chosen similar to the silicon dioxide [16]. The thermocouple conductivity of 1.4 W/(m·K), density of 2200 kg/m^3 and a specific heat of 750 J/(kg·K) were assumed. Only a part of the plate surrounding the thermocouple T_5 was considered.

A square of a side 30 mm was simulated. In the heat conduction model 20 elements were employed in the thickness of the plate. The element size at the cooled surface was only 0.25 mm. In the x_2 and x_3 directions 16 elements were employed. The thermophysical properties of EN 1.4724 steel employed in the heat conduction model have been shown in Fig. 5 and Fig. 6.

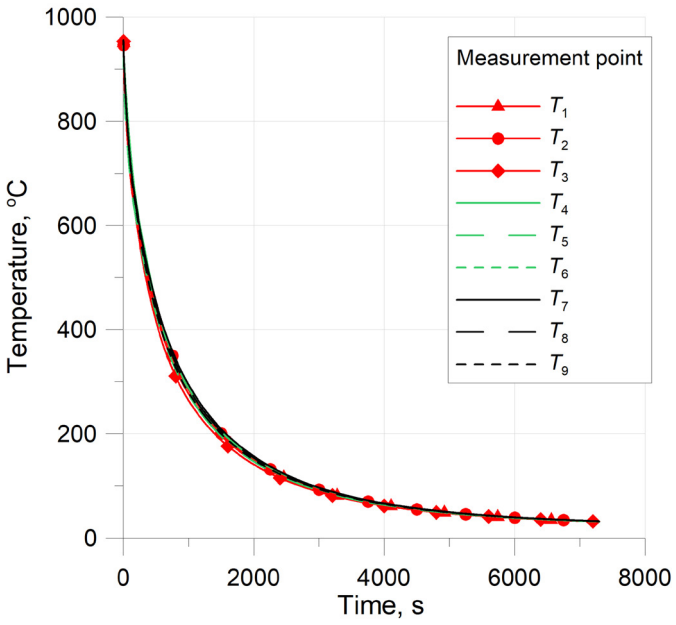

Fig. 3. The plate temperature variations during cooling in the chamber after heating in the electrical furnace to 950°C

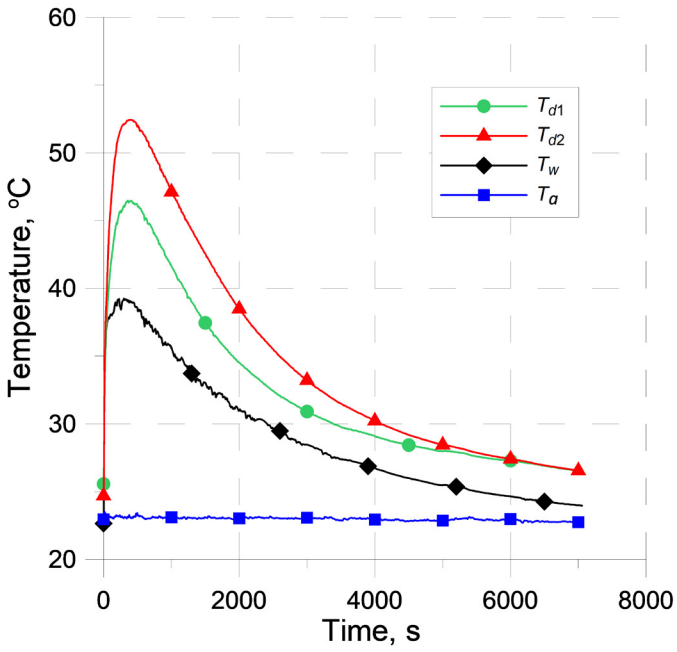

Fig. 4. The chamber temperature variations during the plate cooling

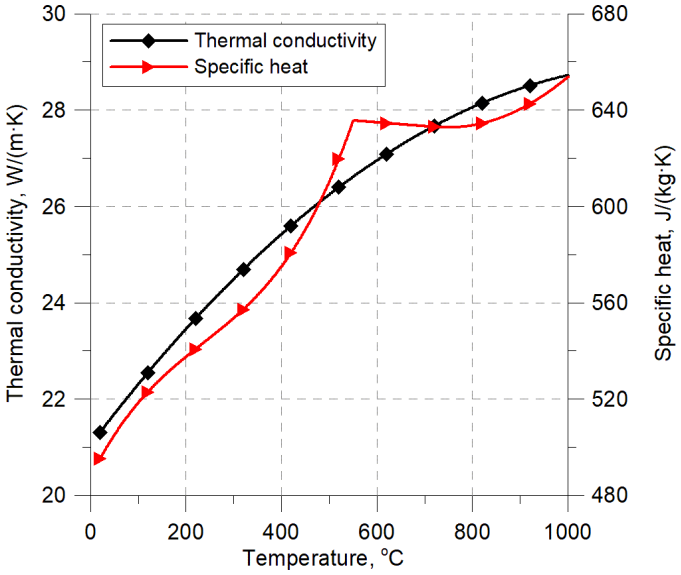

Fig. 5. Specific heat and thermal conductivity as the functions of temperature for EN 1.4724 steel

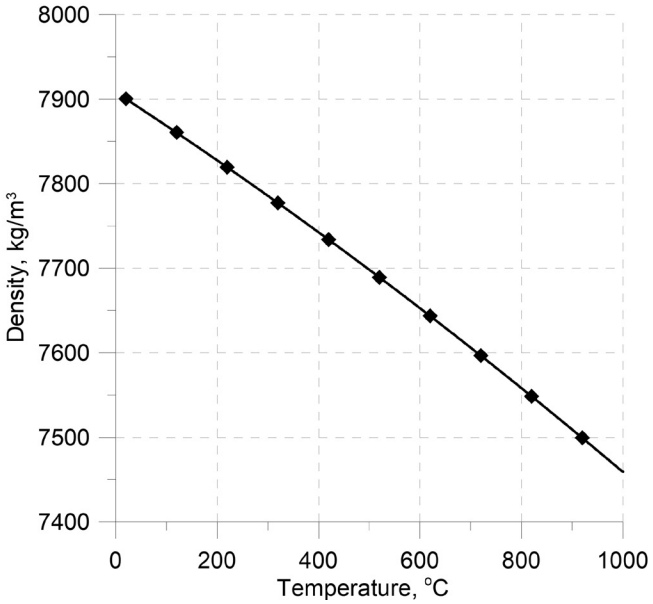

Fig. 6. Density as the function of temperature for EN 1.4724 steel

Thermal conductivity, specific heat and density have been taken from Goldsmith et al. [17]. The radiation and convection heat loss at the plate surface was modeled using the effective heat transfer coefficient. The effective heat transfer coefficient of 100 W/(m^2·K) was specified. It has given the heat flux at the plate surface comparable to that expected at the beginning of plate cooling. At the sides of the modeled part of the plate zero heat fluxes were specified for the simplification of the heat conduction model. The assumed simplifications of boundary conditions and the thermocouple properties and shape could result in some over estimation of the thermocouple influence on the plate temperature. The simulations have shown that the maximum difference in temperature of the plate with and without thermocouple was only 0.7°C. Thus, the cumulated error resulting from the thermocouple accuracy, the gauge accuracy and the inclusion created by the thermocouple was about 4.55°C.

3. The inverse method formulation

In the inverse solution for the heat transfer boundary condition identification, the plate temperature has been computed from the equation

$$\frac{\partial T}{\partial \tau}=\frac{1}{\rho c}\left[\frac{\partial}{\partial x_1}\left(\lambda\frac{\partial T}{\partial x_1}\right)+\frac{\partial}{\partial x_2}\left(\lambda\frac{\partial T}{\partial x_2}\right)+\frac{\partial}{\partial x_3}\left(\lambda\frac{\partial T}{\partial x_3}\right)\right] \quad (1)$$

where:

T – Temperature, K;
x_1, x_2, x_3 – Cartesian coordinates, m;
ρ – Density, kg/m^3;
λ – heat transfer coefficient, W/(m·K);
c – Specific heat, J/(kg·K).

The algorithm and the FEM solver developed by Malinowski et al. [18] was employed to solve Eq. (1). In the FEM solution to Eq. (1) 320 elements with the linear shape functions were employed. The FEM mesh in the x_2-x_3 plane has been shown in Fig. 7. In the thickness of the plate 4 elements were employed. Since the vertical plate was symmetrically cooled from both sides only a half of the plate thickness and length was considered in the FEM model. The FEM mesh showed in Fig. 7 has been selected based on preliminary plate cooling simulations. The plate temperature was modeled using FEM-RE mesh with 1890 elements and the time increment 1s. It allowed to determine the plate temperature at the thermocouple's locations with high accuracy. However, the computation time (CPU) per one simulation was 6.75 s on a PC computer equipped with Intel Core i9-10920X CPU @ 3.50 GHz processor, TABLE 2. Since one inverse solution involving the model V requires about 10000 plate temperature simulations, the CPU time should be reduced if possible. First, the number of elements in x_1 direction has been reduced from 7 to 4 (FEM-R1 mesh). Reduction of the elements number and size did not cause any noticeable error to the temperature field, TABLE 2. Next, the mesh size in x_2 and x_3 direction has been reduced. An increase of a maximum element size from 10 to 15 mm (FEM-R2 mesh) resulted in a minor temperature errors with a maximum deviation of about ±0.6 K. Finally, a minimum element size in x_2 and x_3 direction has been increased to 15mm and 10mm (FEM-R3 mesh), respectively. The maximum temperature errors increased to –0.64/+1.17 K. Since the temperature measurements error was about 4.55 K it can be concluded that the reduced FEM-R3 mesh is sufficient for the inverse solution to the plate cooling in air. The FEM-R3 mesh allowed to reduce the CPU time to 9 hours for one inverse solution with the boundary condition model V. The average temperature error (ATE) has been calculated as a square root of the error norm (5).

The heat flux at the plate surfaces has been approximated using the convection HTC and the plate surface emissivity $\varepsilon_z(T)$

TABLE 2

Summary of FEM tests results

Parameter	Unit	FEM mesh			
		FEM-RE	FEM-R1	FEM-R2	FEM-R3
CPU time	s	6.75	1.45	1.09	0.7
ATE to FEM-RE	K	—	0.008	0.044	0.064
Maximum temperature errors	K	—	–0.02/+0.08	–0.64/+0.60	–0.64/+1.17
Min./Max. element size in x_1 direction	mm	0.5/1.0	1.0/2.0	1.0/2.0	1.0/2.0
Min./Max. element size in x_2 direction	mm	0.5/10	0.5/10	0.5/15	15/15
Min./Max. element size in x_3 direction	mm	0.5/10	0.5/10	0.5/15	10/15
Number of elements		1890	1080	720	320

$$\dot{q}\left(x_1;x_2;x_3;\tau\right) = \\ = 5.67\cdot 10^{-8}\frac{\left[T_p\left(x_1;x_2;x_3,\tau\right)\right]^4-\left[T_k\left(\tau\right)\right]^4}{\frac{1}{\varepsilon_z\left(T\right)}+\frac{S_s}{S_k}\left(\frac{1}{\varepsilon_k}-1\right)}+ \\ +\propto_{con}\cdot\left[T_p\left(x_1;x_2;x_3,\tau\right)-T_a\right] \tag{2}$$

The first term in Eq. (2) describes the radiation heat losses to the chamber walls. The radiation heat transfer was modelled in enclosure consisting of a small convex object (plate) surrounded by a large concave surface (chamber). It was assumed that the surfaces are gray, diffuse, and opaque. The derivation of the radiation model assumed in Eq. (2) can be found in [19]. The radiation model was derived under the assumption that a small object temperature as well as the enclosure temperature is constant. In Eq. (2) the chamber temperature T_k is constant at a particular time τ. The chamber surface temperature $T_k(\tau) = T_w(\tau)$ was specified based on the thermocouple indication placed in the chamber wall parallel to the plate surface, Fig. 4. Moreover, at a particular time τ the plate temperature is nearly constant, Fig. 3. The cooling chamber was made of a stainless steel and had the surface of $S_k = 4.33$ m^2. The sample surface was $S_s = 0.08$ m^2. Since the plate surface was only 1.8% of the chamber surface it was assumed that a radiation heat exchange in the chamber can be described by a model derived for a small object in a large enclosure [19].

The chamber emissivity $\varepsilon_k = 0.2$ was assumed in the boundary condition model. The chamber emissivity was determined comparing the chamber temperature measurements given by the thermal camera with T_w thermocouple. The initial condition was specified based on measurements of the plate temperature after heating.

The plate temperature at a particular time τ varies slightly in x_2 and x_3 directions, Fig. 3. It has been assumed that the convection HTC can be approximated by a second-degree polynomials with a sufficient accuracy. For that, the convection HTC over the vertical plate surface has been approximated using only one surface element with the parabolic shape functions N_i

$$\propto_{con}\left(x_2,x_3,\tau\right) = \sum_{i=1}^{8} N_i\left(\xi_2,\xi_3\right)\sum_{j=1}^{4} G_j\left(\xi_1\right)\propto_{ij} \tag{3}$$

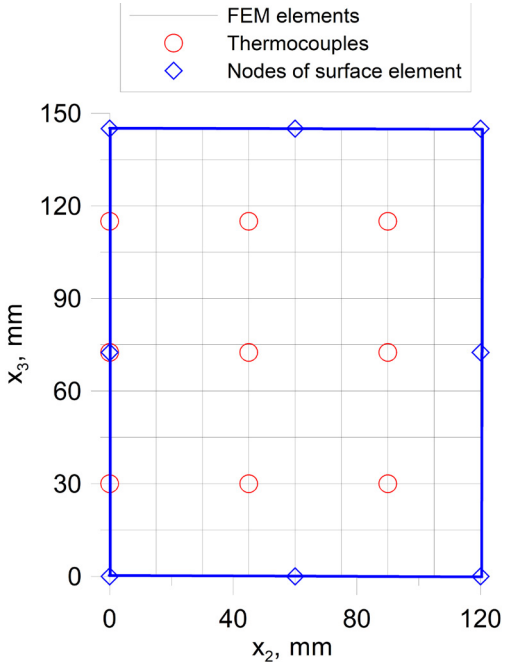

Fig. 7. Finite element mesh FEM-R3, location of the thermocouples and nodes of the surface element employed in the boundary condition model V

In Eq. (3) ξ_2, ξ_3 are natural coordinates of the surface element on the interval (–1, 1). The parabolic shape functions N_i can be found in [20]. The first term in Eq. (3) describes the convection HTC distribution over the plate surface at a particular time τ. But the HTC varies in time as well. For that, the HTC distribution in time at nodes of the surface elements has been interpolated with the cubic shape functions G_j [20]. The coordinate ξ_1 in Eq. (3) denotes the dimensionless time

$$\xi_1 = \frac{2\tau-\tau_1-\tau_2}{\tau_2-\tau_1} \tag{4}$$

In Fig. 7 the division of the plate into FEM linear elements and the surface element covering the vertical plate surface have been presented. In the case of one surface element the HTC variations at 8 nodes must be determined to describe the HTC distribution over the plate surface as well as in time. The time of cooling was divided into KT intervals. The unknown $\propto_{ij}$ coefficients were grouped in a vector p_i of a length $N_{HTC} = 8\cdot(KT\cdot 3 + 1)$. The

number of time intervals depends on the problem of cooling. The implemented inverse solution strategy was described by Hadała et al. [21]. The coefficient defining the unknown boundary condition at the plate surface has been determined from the minimum condition of the error norm

$$E(p_i)=\frac{1}{NT\,NP}\sum_{m=1}^{NT}\sum_{n=1}^{NP}\left(Te_n^m-T(p_i)_n^m\right)^2 \tag{5}$$

where:

Te_n^m – Sample temperature measured by the sensor n at the time τ_m;

T_n^m – Computed sample temperature at the location of the sensor n at the time τ_m;

NP – Number of temperature sensors;

NT – Number of temperature measurements performed by one sensor.

The inverse solution can give the boundary condition at the vertical plate surface if the boundary conditions at the other plate surfaces are known. At the temperature symmetry planes zero heat fluxes have been specified

$$\dot{q}(x_1;x_2=0;x_3)=-\lambda\frac{\partial T}{\partial x_2}=0 \tag{6}$$

$$\dot{q}(x_1=0;x_2;x_3)=-\lambda\frac{\partial T}{\partial x_1}=0 \tag{7}$$

At the plate edges the convection heat losses have been approximated using the Nu models. At the vertical edge of the plate the Nusselt number Nu has been computed from the formula given by Churchill et al. [14] using an equation (15).

At the horizontal edge of the plate cooled from the above the formula developed by Lewandowski et al. [22] has been employed

$$Nu=0.774\,Ra^{1/5} \tag{8}$$

where:

Ra – Rayleigh number ($Ra = Gr \cdot Pr$),

Pr – Prandtl number.

At the horizontal edge of the plate cooled from the bottom the Nusselt number has been calculated from the formula given by Aihara et al. [23]

$$Nu=0.5Ra^{1/5} \tag{9}$$

The minimization of the error norm (5) was accomplished using the Broyden-Fletcher-Goldfarb-Shanno (BFGS) algorithm. The BFGS formula was proposed independently by Broyden [24], Fletcher [25], Goldfarb [26] and Shanno [27]. The BFGS algorithm builds up, iteratively, the Hessian matrix based on the objective function derivatives

$$\frac{\partial E(p_i)}{\partial p_j}\approx\frac{E(p_i+\Delta p_j)-E(p_i)}{\Delta p_j} \tag{10}$$

The increment $\Delta p_j = |p_j|\ 10^{-6}$ has been used in forward estimation of the partial derivatives. Three stopping criteria have been used to terminate the minimization procedure. The first controls a decrease in the objective function value $DE = E(p_j)^k - E(p_j)^{k-1}$. The second criterion controls an average value of the objective function derivatives with respect to optimized parameters:

$$DG=\frac{1}{N_{HTC}}\sum_{j=1}^{N_{HTC}}\left|\frac{\partial E(p_i)}{\partial p_j}\right| \tag{11}$$

The minimization procedure was terminated if DE or DG was lower than EPS in the two subsequent minimization steps k and $k-1$. For all the solutions EPS = $1.0\cdot10^{-8}$ have been specified. The third criterion limits a number of iterations allowed for updating the Hessian matrix. It is known that the BFGS updating formula is efficient up to N iteration. Where N denotes a number of unknown parameters to be determined. Thus, a maximum number of iterations was set to N_{HTC} for the considered case. However, to reach the accuracy defined by the criterion (10) or (11) it was necessary to complete about 10 minimizations of the error norm. The solution obtained from the last minimization (p_i vector) served as a starting point for the next optimization. More about the BFGS algorithm and nonlinear optimization methods can be found in [28].

4. Models of the boundary condition at the plate surface

The inverse solution has given the heat flux distribution at the vertical plate surface. It has allowed to calculate the average heat flux

$$\dot{q}_{avg}=\frac{\int_{x_2=0}^{x_2=0.12}\int_{x_3=0}^{x_3=0.145}\dot{q}(x_2,x_3)\,dx_2dx_3}{S_{hp}},\mathrm{W/m^2} \tag{12}$$

The average plate surface temperature has been calculated from

$$T_p=\frac{1}{S_{hp}}\int_{x_2=0}^{x_2=0.12}\int_{x_3=0}^{x_3=0.145}T_p(x_2,x_3)\,dx_2dx_3,\mathrm{°C} \tag{13}$$

Where the vertical plate surface was $S_{hp} = 0.0174$ m^2.

The average heat flux $\dot{q}_{avg}$ at the vertical plate surface S_{hp} was used for the determination of the accuracy of the local models which define the heat losses due to convection and radiation at the vertical plate surface as well as at the vertical edge of the plate. Depending on the α_{con} and the plate surface emissivity $\varepsilon_z(T)$ three models of the boundary condition at the vertical plate surface were tested.

4.1. Natural convection models

Three models of the natural convection at the vertical plate surface were examined and tested. The convection HTC has been calculated from

$$\alpha_{con} = \frac{Nu\,L}{\lambda_a} \tag{14}$$

Where: L – Characteristic length, $L = 0.145$ m for the vertical plate. The thermal conductivity of air λ_a was calculated at the ambient temperature T_a. The air properties necessary to calculate the Ra and Pr numbers have been calculated at the ambient temperature T_a.

4.1.1. Model 1

The heat losses due to convection has been computed from the equation developed by Churchill et al. [14]

$$Nu = \left\{ 0.825 + \frac{0.387 Ra^{1/6}}{\left[1 + \left(0.492 / Pr\right)^{9/16}\right]^{8/27}} \right\}^2 \tag{15}$$

4.1.2. Model 2

The model 2 utilizes the relation proposed by Churchill and Chu

$$Nu = \left\{ p_4 + \frac{p_5 Ra^{p_7}}{\left[1 + \left(p_6 / Pr\right)^{p_8}\right]^{p_9}} \right\}^2 \tag{16}$$

However, the coefficients: $p_4, \ldots, p_9$ have been determined from the error norm minimization.

4.1.3. Model 3

The heat losses due to convection has been computed from the exponential function

$$Nu = p_4 Ra^{p_5} \tag{17}$$

The coefficients: p_4 and p_5 have been determined from the error norm minimization.

4.2. Emissivity model

The boundary condition model (2) combines the natural convection and radiation heat losses over the vertical plate surface. In the radiation model it was assumed that the emissivity depends on temperature

$$\varepsilon_z = p_1 + p_2 \bar{t}_p + p_3 \bar{t}_p^2 \tag{18}$$

The model (18) describes the plate surface emissivity as a parabolic function of the dimensionless temperature $\bar{t}_p = T_p(x_1, x_2, x_3)/1200°C$.

5. The uncertainty of the inverse solution

It has been mentioned in the section 3 that the inverse solution has been formulated as a nonlinear optimization problem. The inverse matrix (Hessian matrix) is built up iteratively. It is rather simply to prove that the solution (p_i vector) is correct for the exact temperature indications at specified points (for example at the thermocouple locations). However, the temperature measurements are subjected to errors which can result in the inverse solution inaccuracy to the boundary condition. It is important to determine the level of the inverse solution uncertainty related to the temperature measurement errors. The accumulated error resulting from the thermocouple accuracy, the gauge accuracy and the inclusion created by the thermocouple was described in the section 2. Its maximum value was estimated at a level of 4.55°C. Thus, the simulated thermocouple's readings should exhibit similar errors. It is known that the temperature measurements errors depend on the temperature value. Thus, the highest temperature errors should be achieved at the beginning of cooling. Moreover, the simulated temperature errors should decrease in time. To avoid a numerical bias, it is important to simulate the thermocouples readings based on the numerical solution to the heat conduction problem different from that employed in the objective function minimization. For that the plate temperature was simulated using a nonlinear FEM solver. The employed nonlinear FEM solver utilizes a third-degree shape functions instead of linear shape functions described as FEM-R3 mesh. Only four nonlinear elements over the entire domain shown in Fig. 7 has been used to achieve a lower solution accuracy to the temperature field. The employed nonlinear FEM solver was described in [18]. The nonlinear FEM solver had shown a maximum temperature error of 5.7°C in comparison to the solution obtained with the linear FEM-R3 mesh shown in Fig. 7. In order to generate a simulated temperature readings, at the plate edges the boundary condition described in the section 3 were specified. At the vertical plate surfaces the boundary condition developed by Churchill et al. [14] has been used (the model 1) as a test function to be retrieved from the inverse solution. Further, for the simulated temperature indications the plate emissivity $\varepsilon_z = 0.6$ was specified. It is expected that the inverse solution gives a similar plate emissivity simultaneously determined with the convection HTC.

It has been mentioned that the simulated temperature readings have shown a maximum temperature error of about 5.7°C. The imposed errors on the synthetic thermocouple indications varied in time and space. At the thermocouple 9 the highest positive deviation has been observed, while at the thermocouple 5 the highest negative deviation has been noticed. The simulated temperature measurements errors vanished in time as the plate temperature decreased, Fig. 8. Similar distribution of the temperature measurements errors is expected in the physical experiment.

The inverse solution to the simulated temperature readings should give the convection HTC defined by the model 1 and the plate emissivity $\varepsilon_z = 0.6$. The results of the uncertainty tests have been summarized in TABLE 3 and shown in figures from 9 to 11. The plate initial temperature was 950°C. The average heat flux

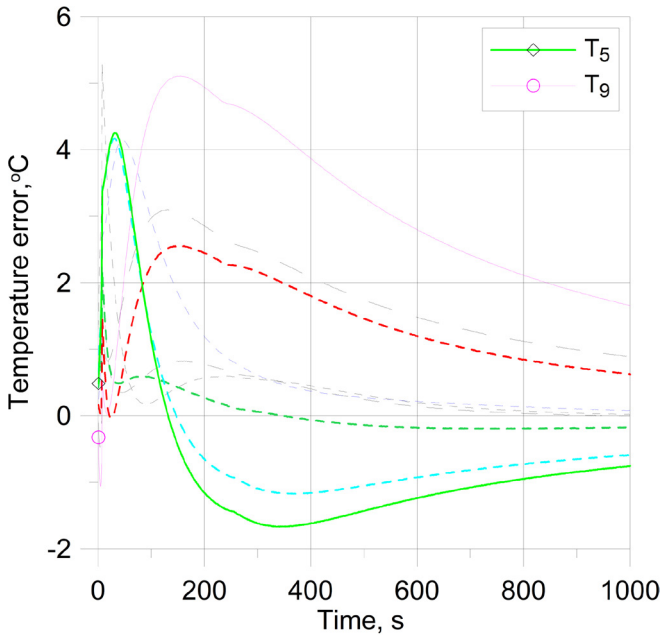

Fig. 8. Simulated temperature measurements errors at the location of the thermocouple 5 and 9

at the plate surface computed from the model 1 (test function to be retrieved) has been plotted in figures as the solid red line. The inverse solutions to the average heat flux $\dot{q}_e$ have been plotted in Fig. 9 as the dotted lines. All the models have given a good approximation to the heat flux distribution versus the average plate surface temperature. The heat flux curves nearly overlapped the test function (the model 1). Some minor errors of the inverse solutions to the heat flux have been summarized in TABLE 3. The maximum error to the average heat flux did not exceed 5%.

The model 2 had the same form as the test function (the model 1) but the coefficients defining the Nusselt number were

TABLE 3

Accuracy of the inverse solutions to the heat flux and temperatures

Parameter	Unit	Inverse solution utilizing boundary condition model:		
		Model V	Model 2	Model 3
Average error to heat flux $\dot{q}_{avg}$	kW/m^2	0.013	0.005	0.059
Maximum error to heat flux $\dot{q}_{avg}$	kW/m^2	0.97	0.29	3.33
	%	1.2	0.3	4.1
Average temperature error	K	0.23	0.25	1.1
Maximum temperature error	K	5.6	5.9	6.5

computed from the error norm minimization. Due to the errors introduced to the simulated temperature measurements the inverse solution was shifted slightly from the original model 1. The differences to the heat flux were low with the maximum value below 0.5%. The maximum temperature errors were at a level of the temperature measurements errors. The convection HTC, Fig. 10, and the plate surface emissivity, Fig. 11, have been reproduced correctly. Thus, the invers solution utilizing the model 2 has given nearly a mirror of the specified emissivity and the convection HTC.

The model 3 uses the McAdams type formula and has a slightly different nonlinearity from the test function (the model 1). It has resulted in an error of 20% to the convection HTC at higher temperatures, Fig. 10. The solution to the average heat flux obtained from the McAdams formula was much better with an error of 4%, TABLE 3. A better solution to the heat flux in comparison to the convection HTC has resulted from an overestimation of the plate surface emissivity of about 7.5%, Fig. 11. Thus, the decomposition of the heat flux into the convection and radiation part was not correct in the case of model 3.

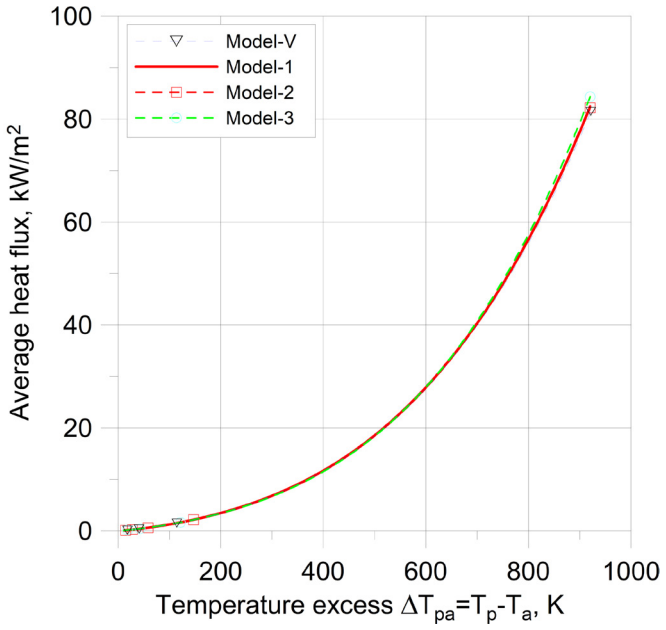

Fig. 9. Comparison of the inverse solutions to the specified heat flux (Model 1)

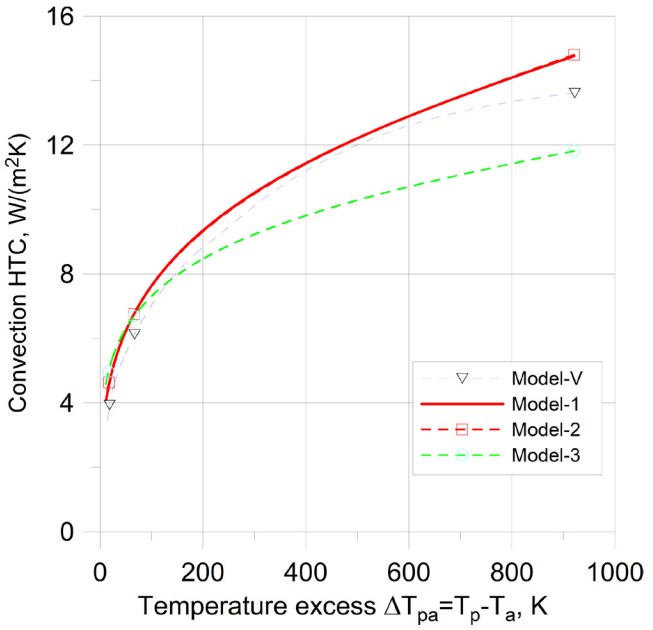

Fig. 10. Comparison of the inverse solutions to the specified convection HTC (Model 1)

The best solution to the temperature field has given the model V. The model has been designed to identify the plate emissivity and the convection HTC over the plate surface for an unknown regime of air flow. For the considered test, two periods of time were employed in the boundary condition model defined by Eq. (3). It gave $N_{HTC} = 56$ coefficients defining the convection HTC. In addition to that, three coefficients defining the plate emissivity in Eq. (18) have been added to the vector p_i. It gave $N = 59$ parameters which have been determined from the minimum condition of the error norm (5). The model gave ATE = 0.23°C over the entire range of the plate temperature. The maximum error to the heat flux was below 1.5%. The model V was capable to decompose the convection HTC and the plate surface emissivity, Fig. 11. The models 2 and 3 based on the closed form equations are not capable of varying the convection HTC over the plate surface depending on the local flow of air. For that reason, the inverse solutions to the measured temperatures may be less accurate in the case of these models. The model V has allowed for the convection HTC variation over the plate. Further, no assumption was made concerning the convection HTC variation versus the plate temperature. The model V can serve as the reference solution for the heat flux and emissivity. It allows the comparison of the other models' accuracy in inverse solutions to the physical experiment of the plate cooling. Notice that the emissivity model has been tested in the uncertainty tests. The simulated temperature histories were obtained for a constant emissivity of $\varepsilon_z = 0.6$. Thus, the inverse solutions did not introduce nonlinearity to the plate surface emissivity in the case of simulated temperature readings.

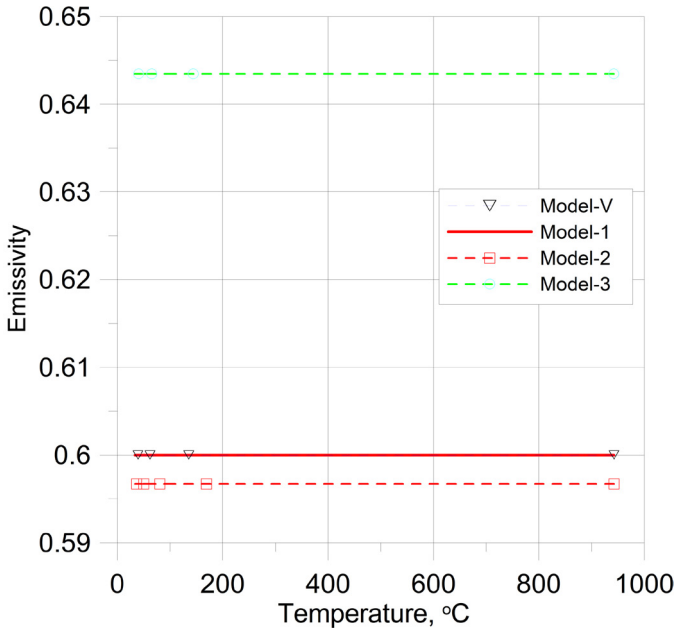

Fig. 11. Comparison of the inverse solutions to the specified (Model 1) plate surface emissivity

6. The results of heat flux and heat transfer coefficient identification

The inverse solutions were performed by minimizing the error norm (5) for the measured temperatures which have been shown in Fig. 3. The chamber temperature $T_k(\tau)$ was specified according to the measured temperature of the chamber wall parallel to the plate surface depicted in Fig. 4 as the T_w curve. The inverse solutions gave the average temperature errors ATE varying from 1.8 to 4.2°C. The ATE have been summarized in TABLE 4 for the simultaneous determination of the convection HTC as well as the plate emissivity defined by Eq. (18).

TABLE 4

The average temperature errors (ATE) of the inverse solutions to the measured temperatures

Model number	ATE °C
V	1.8
1	4.1
2	4.2
3	4.1

In Fig. 12 the plate temperature indicated by the thermocouple 5 has been compared to the plate temperatures computed from the HTC models and the plate emissivity model defined by Eq. (18). For the plate surface emissivity approximated by a second-degree polynomial, the models 1, 2 and 3 have given similar errors. It must be pointed out that in the case of model 1 none of the parameters describing the convection HTC was determined from the error norm minimization. Only parameters describing the plate surface emissivity were optimized. The optimization of the *Nu* models' parameters has led to similar ATE and the computed and measured temperatures nearly overlapped. However, good agreement of the temperatures histories indicates only that the heat flux at the plate surface was correctly identi-

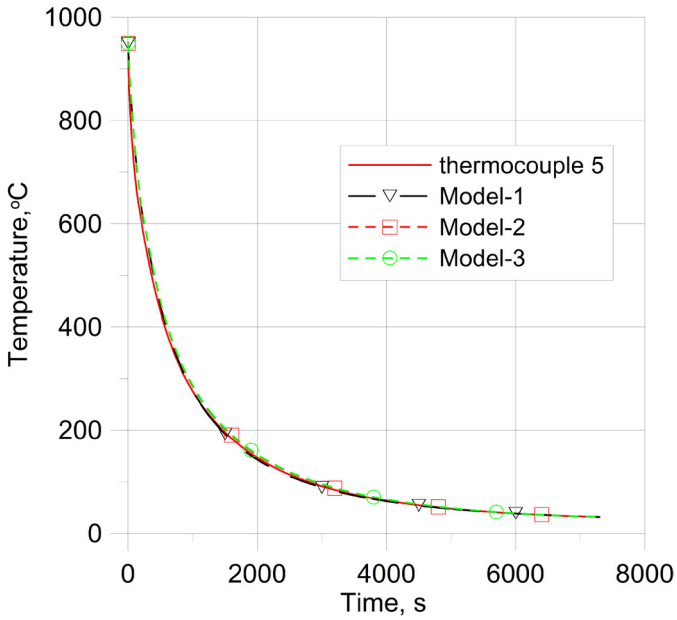

Fig. 12. Comparison of the temperature history indicated by the thermocouple 5 with the inverse solutions based on the tested models of heat convection and emissivity

fied. An essential error may result in the decomposition of the radiation and convection part of the heat flux.

The lowest ATE = 1.8°C has given the model V which has been considered as the reference solution to the heat flux and emissivity at the vertical plate surface. For the measured temperatures, five periods of time were employed in the boundary condition model defined by Eq. (3). It gave N_{HTC} = 88 coefficients defining the convection HTC. In addition to that, three coefficients defining the plate emissivity in Eq. (18) have been added to the vector p_i. It gave $N = 91$ parameters which have been determined from the minimum condition of the error norm (5).

As the plate temperature grows the radiation heat losses are more and more important and the convection Nu models were extended with the radiation model (18). In the inverse solutions the polynomial coefficient in Eq. (18) as well as the Nusselt number coefficients were determined from the error norm minimization. The obtained parameters have been given in TABLE 5. Notice that in the case of model 1 parameters: p_4, …, p_9 were not optimized and had values proposed by Churchill et al. [14].

TABLE 5

The parameters of the Nusselt number and the emissivity model (18) obtained from the error norm minimization

Parameter	Model 1	Model 2	Model 3
p_1	0.704	0.424	0.390
p_2	–1.400	0.159	0.122
p_3	1.958	0.244	0.134
p_4	0.825	2.103	2.613
p_5	0.387	1.334	0.172
p_6	0.492	0.664	—
p_7	0.166	$7.603 \cdot 10^{-2}$	—
p_8	0.562	0.514	—
p_9	0.296	$1.498 \cdot 10^{-2}$	—

The Nu based models were compared with the reference model V, and the possibilities of the simultaneous determination of the convection and radiation heat losses were discussed. The heat flux predicted by all the models has agreed well with the reference model V, Fig. 14. But the convection part decomposed from the total heat flux is different, Fig. 13. For example, the difference between the model V and the Churchill and Chu formula (Model 1) was about 10 kW/m^2 at 800°C. Optimization of the Nu parameters in the Churchill and Chu formula (Model 2) as well as in the McAdams formula (Model 3) did not change the convection heat flux essentially, Fig. 13. Thus, good prediction of the total heat flux by *Nu* models was due to the plate emissivity overestimation, Fig. 15. The surface emissivity predicted by the model 1 had a minimum value of 0.45 at 430°C (Fig. 15). But at the ambient temperature as well as at 800°C the emissivity was about 0.7. Such variation of the plate emissivity is not supported by the experiments performed by Burakowski [2] for this grade of steel.

The minimization of the parameters defining the convection and radiation heat losses in the model 2 and model 3 has given a similar plate surface emissivity growing from about 0.4 at the ambient temperature to about 0.65 at 800°C. Thus, simultaneous minimization of the parameters defining the Nu number, Fig. 16, and the plate emissivity, Fig. 15, has given qualitatively correct decomposition of the total heat flux. However, the emissivity is too high in view of the results published by Burakowski [2]. Moreover, in the case of Nu models, the ATE of about 4 K was high as for the plate cooling in air, Table 4. It means that the convection HTC computed from Eq. (16), or Eq. (17) was not sufficiently exact for the decomposition of the total heat flux into radiation and convection part. The emissivity obtained from the model V was close to 0.25 at 300°C and 0.48 at 800°C as reported by Burakowski [2]. Since the emissivity

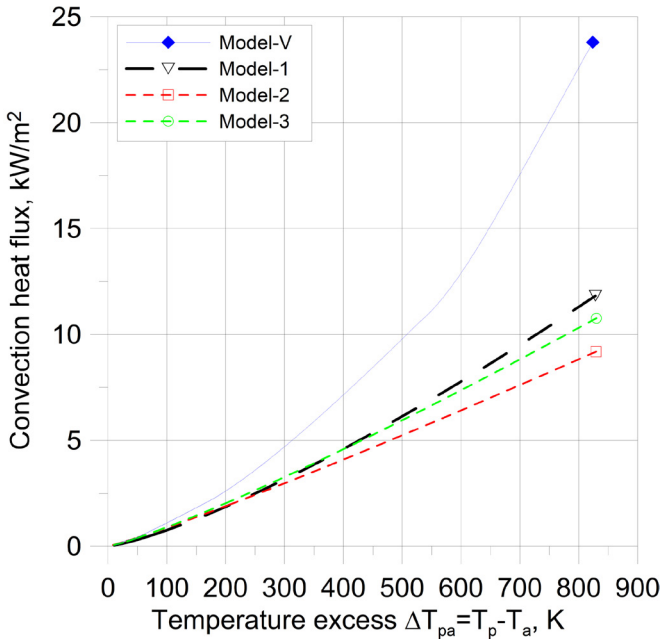

Fig. 13. The convection heat flux determined from the models compared to the reference model V

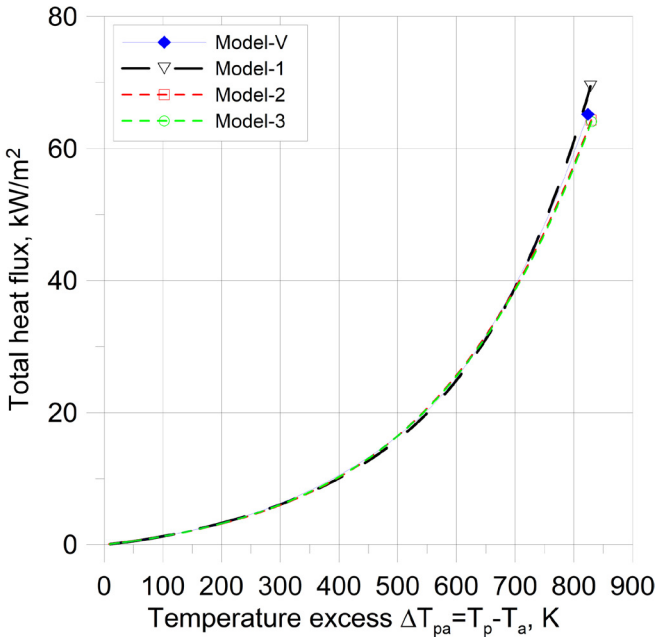

Fig. 14. The total heat flux determined from the models compared to the reference model V

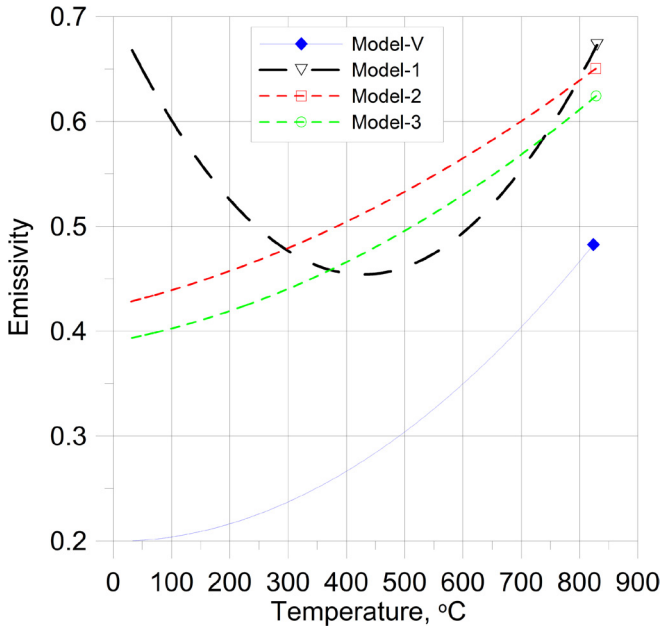

Fig. 15. Emissivity determined from the models compared to the reference model V

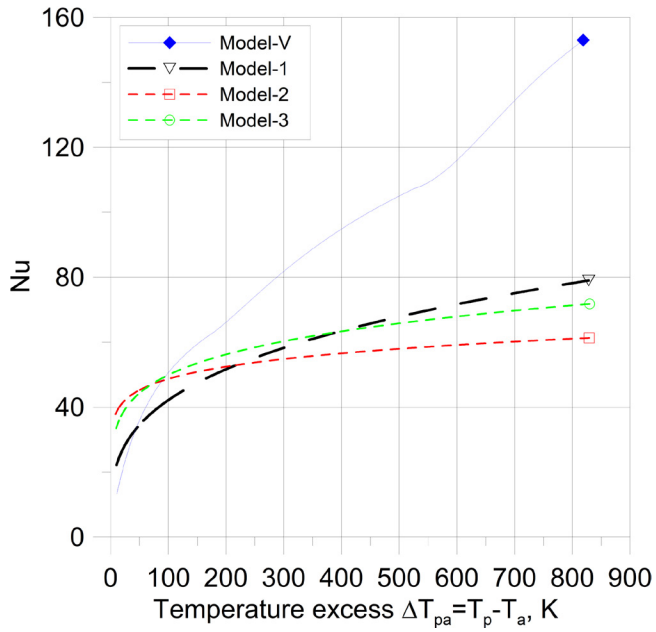

Fig. 16. The Nusselt number obtained from the models compared to the reference model V

has been correctly identified and the lowest temperature error has been obtained for the model V, thus the convection part has the best accuracy in the case of V model. The course of the Nusselt number change obtained from the V model in relation to the other models indicates an essential increase in the *Nu* number for temperatures above 100°C (Fig. 16). However, the model V has required 91 parameters to be determined instead of 9 (Model 2), or 5 (Model 3).

7. Conclusions

In the case of temperature reaching 900°C, at the initial stage of cooling in air an important role has the radiation heat loss. The separation of the convection and radiation parts is difficult due to the simultaneous influence of both mechanisms on the plate temperature. It requires the accurate determination of the surface emissivity. The other choice is to limit the radiation heat loss as low as possible at the experimental stand. It is possible for polished surfaces at low temperatures. Metals heated to high temperature oxidized and emissivity grows. Moreover, the boundary layer depends on the surface roughness. Thus, determination of the convection heat losses for cooling plates having a natural surface roughness would be important for practice. It has been shown that it is possible but required a high accuracy model describing the convection heat loss. The Nu models based on the Churchill and Chu, or McAdams's formula did not reach the required accuracy. The polynomial approximation of the convection HTC has given the desired accuracy, but the number of unknown parameters reached 88. The determined surface emissivity has varied from 0.2 at room temperature to about 0.47 at 800°C. The obtained emissivity from the model V was in good agreement to the measured values obtained by Burakowski for the same grade of steel. The inverse solution from the model V has allowed for accurate identification of the heat flux for the surface emissivity depending on the plate temperature. The comparison of the identified convection heat loss has shown the lowest differences to the boundary condition proposed by Churchill et al. [14] for the air properties calculated at the ambient temperature. However, at 800°C the difference was essential.

The identified values of the Nusselt number parameters, that allow to determine the convective boundary condition (model 2, TABLE 4), can be used for cooling vertical plates in the high temperature range. These problems are most often encountered during plastic forming processes, e.g. hot forging, rolling or continuous casting.

Acknowledgements

This work was supported by the regular activity of the Faculty of Metals Engineering and Industrial Computer Science of AGH University of Science and Technology (Work No. 16.16.110.663).

REFERENCES

[1] A. Wrożyna, M. Pernach, R. Kuziak, M. Pietrzyk, JMEP **25**, 2016-1481 (2016). DOI: https://doi.org/10.1007/s11665-016-1907-9

[2] T. Burakowski, Metaloznawstwo i Obróbka cieplna **3**, 31-40 (1973).

[3] G. Béranger, G. Henry, G. Sanz (Ed.), The book of steel, Intercept Limited, Andover Hampshire U.K. (1996).

[4] F. Puschmann, S. Eckehard, Exp. Therm. Fluid Sci. **28**, 607-615 (2004).
DOI: https://doi.org/10.1016/j.expthermflusci.2003.09.004

[5] Q. Bai, J. Lin, L. Zhan, T.A. Dean, D.S. Balint, Z. Zhang, Int. J. Mach. Tool Manuf. **56**, 102-110 (2012). DOI: https://doi.org/10.1016/j.ijmachtools.2011.12.005

[6] S. Shamasundar, A.A. Tseng, W. Aung, J. Mater. Process. Technol. **36**, 199-221 (1993). DOI: https://doi.org/10.1016/0924-0136(93)90031-Z

[7] B. Hadała, Int. J. Therm. Sc. **71**, 172-181 (2013). DOI: https://doi.org/10.1016/j.ijthermalsci.2013.04.012

[8] Z.Malinowski, A. Cebo-Rudnicka, T. Telejko, B. Hadała, A. Szajding, Inverse Probl. Sci. Eng. **23**, 518-556 (2015). DOI: https://doi.org/10.1080/17415977.2014.923417

[9] Z. Malinowski, J.G. Lenard, M.E. Davies, J. Mat. Proc. Tech. **41**, 125-142 (1994). DOI: https://doi.org/10.1016/0924-0136(94)90057-4

[10] C. Devadas, IV. Samarasekera, Ironmaking and Steelmaking **13**, 311-321 (1986).

[11] E. Eckert, T. Jackson, NACA Tech. Rep. (1951).

[12] W.H. McAdams, Heat Transmission, McGraw-Hill, New York (1954).

[13] M. Schaub, M. Kriegel, S. Brandt, Int. J. Heat Mass Trans. **136**, 1186-1198 (2019). DOI: https://doi.org/10.1016/j.ijheatmasstransfer.2019.03.089

[14] S.W. Churchil, H.H.S. Chu, Int. J. Heat Mass Trans. **18**, 1323-1329 (1975). DOI: https://doi.org/10.1016/0017-9310(75)90243-4

[15] K. Cao, J. Baker, Int. J. Heat Mass Trans. **90**, 26-33 (2015). DOI: https://doi.org/10.1016/j.ijheatmasstransfer.2015.05.014

[16] A.Ç. Yunus, Heat and mass transfer. McGraw-Hill, New York (2007).

[17] A. Goldsmith, T.E. Waterman, H.J. Hirschhorn, Handbook of thermophysical properties of solid materials, vol. 2, Pergamon Press, New York (1962).

[18] Z. Malinowski, T. Telejko, B. Hadała, A. Cebo-Rudnicka, A. Szajding, Int. J. Heat Mass Trans. **75**, 347-361 (2014). DOI: https://doi.org/10.1016/j.ijheatmasstransfer.2014.03.078

[19] J.P. Holman, Heat Transfer, McGraw-Hill, New York (2010).

[20] O.C. Zienkiewicz, R.L. Taylor, The Finite Element Method, vol. 1: The Basis, Butterworth-Heinemann, Linacre House, Oxford OX2 8DP, Jordan Hill (2000).

[21] B. Hadała, Z. Malinowski, T. Telejko, A. Szajding, A. Cebo-Rudnicka, Int. J. Therm. Sci. **136**, 200-216 (2019). DOI: https://doi.org/10.1016/j.ijthermalsci.2018.10.026

[22] W.M. Lewandowski, E. Radziemska, M. Buzuk, H. Bieszk, Applied Energy **66**,177-197 (2000). DOI: https://doi.org/10.1016/S0306-2619(99)00024-0

[23] T. Aihara, Y. Yamada, S. Endo, Int. J. Heat Mass Trans. **15**, 2539-2549 (1972). DOI: https://doi.org/10.1016/0017-9310(72)90145-7

[24] C.G. Broyden, J. Inst. Math. Appl. **6**, 222-231(1970). DOI: https://doi.org/10.1093/imamat/6.3.222

[25] R. Fletcher, The Computer Journal **13**, 317-322 (1970). DOI: https://doi.org/10.1093/comjnl/13.3.317

[26] D. Goldfarb, Math. Comput. **24**, 23-26 (1970). DOI: https://doi.org/10.1090/S0025-5718-1970-0258249-6

[27] D.F. Shanno Math. Comput. **24**, 647-656 (1970). DOI: https://doi.org/10.2307/2004840

[28] W.H. Press, S.A. Teukolsky, W.T. Vetterling, B.P. Flannery, Numereical Recipes in Fortran 77. The Art of Scentific Computing, Cambrdge University Press, Cambridge (1992).